Am J Cancer Res 2026;16(6):2651-2670
www.ajcr.us /ISSN:2156-6976/ajcr0173518

Original Article

A multimodal imaging-based decision tree for preoperative axillary risk stratification in breast cancer: a retrospective clinical utility analysis

Youjia Hong[1*], Xue Ding[2*], Haiqing Huang[1], Zhe Chen[1], Cong Chen[1], Mumin Wu[1], Sen Jiang[3], Yangkang Li[3]

[1]Department of Ultrasound, Cancer Hospital of Shantou University Medical College, Shantou 515000, Guangdong, China; [2]Department of Medical Imaging, Beijing Corps Hospital, Chinese People's Armed Police Forces, Beijing 100027, China; [3]Department of Radiology, Cancer Hospital of Shantou University Medical College, Shantou 515000, Guangdong, China. [*]Equal contributors.

Received April 23, 2026; Accepted June 7, 2026; Epub June 15, 2026; Published June 30, 2026

Abstract: To evaluate the clinical utility of a preoperative multimodal imaging-based decision tree for axillary risk stratification in breast cancer and to explore its associations, in a retrospective manner with axillary management patterns and short-term postoperative outcomes. This retrospective single-center study included 204 women with primary breast cancer who underwent surgery between January 2023 and December 2024. Preoperative breast MRI and axillary ultrasound performed within 2 weeks before surgery were reviewed in a blinded manner. Postoperative paraffin pathology served as the reference standard for axillary lymph node metastasis (ALNM). Imaging variables associated with ALNM were identified by multivariable logistic regression, and a CART decision tree was constructed for preoperative risk stratification. Model discrimination was evaluated in the overall cohort and in randomly split training and validation sets. Retrospective analyses were further performed to examine the associations of model-defined risk strata with actual axillary surgical management, postoperative morbidity, and 1-year disease-free survival (DFS). Five imaging variables were associated with ALNM: lesion margin morphology, RI, lymph node hilum integrity, lymph node microcalcification, and Adler blood flow grade. The decision tree showed moderate discriminative ability, with an AUC of 0.829 in the overall cohort and AUCs of 0.835 and 0.803 in the training and validation sets, respectively. Model-defined risk strata showed a stepwise increase in the observed rate of ALNM and were retrospectively associated with different patterns of axillary surgery and postoperative morbidity. Exploratory survival analyses based on 1-year follow-up did not support definitive conclusions regarding benefit from postoperative adjuvant therapy. In conclusion, a decision tree derived from routine preoperative breast MRI and axillary ultrasound features may serve as an interpretable tool for preoperative axillary risk stratification in breast cancer. Its potential relevance to axillary management should be interpreted as exploratory and hypothesis-generating, and prospective multicenter validation is required before clinical decision support can be considered.

Keywords: Breast cancer, axillary lymph node metastasis, preoperative risk stratification, breast MRI, axillary ultrasound, decision tree, clinical utility

Introduction

Breast cancer (BC) is the most prevalent malignant tumor among women worldwide. In 2023, approximately 409,000 new cases of BC were diagnosed among Chinese women, and the annual incidence has increased by 3.1% [1]. Axillary lymph node metastasis (ALNM) status is a core indicator for BC TNM staging, prognosis evaluation and individualized treatment strategy formulation, and 30% to 40% of newly diagnosed patients have already developed ALNM at initial consultation [2]. Therefore, a dependable, non-invasive preoperative assessment of ALNM is clinically important, because it influences surgical planning, adjuvant treatment decisions, and prognosis estimation. At present, the gold standard for assessing axillary lymph node status in clinical practice still relies on sentinel lymph node biopsy (SLNB) or axillary lymph node dissection (ALND). However, domestic studies have

https://doi.org/10.62347/VNOA8244

shown that more than 40% of patients who undergo SLNB are pathologically negative after surgery. These patients are exposed to unnecessary surgical trauma and may subsequently develop upper-extremity lymphedema, sensory disturbance, and restricted shoulder mobility, all of which can impair long-term quality of life [3]. When surgical planning is based mainly on experience-driven interpretation of imaging findings, both potentially avoidable invasive axillary intervention and undertreatment of the axilla can easily occur. Accordingly, a noninvasive, standardized, and quantitative tool for preoperative axillary evaluation is needed.

Currently, axillary ultrasound and multimodal breast magnetic resonance imaging (MRI) are the core imaging modalities for preoperative ALNM assessment in clinical practice [4]. Previous studies have shown that conventional axillary ultrasound has a sensitivity of 50%-70% for ALNM assessment and remains limited in detecting micrometastases, deep-seated lesions, and metastatic foci with atypical morphology [5]. Multimodal breast MRI provides high soft-tissue contrast and can improve sensitivity; however, reactive lymph node enlargement and inflammatory hyperplasia may be difficult to distinguish from metastatic involvement on imaging, which can lead to false-positive nodal interpretations [6]. In routine reporting, ultrasound and MRI are often reviewed in combination, but the final weighting of findings across modalities still depends heavily on the individual reader, and a standardized quantitative scheme for cross-modality integration is not commonly used. In addition, conventional statistical modeling is often challenged by high-dimensional imaging descriptors and non-linear feature interactions, which limits the reproducible extraction of complementary information from the two modalities [7].

Machine learning offers an approach to combine multimodal imaging features within a single quantitative model [8]. Decision trees, as supervised learning classifiers, recursively split the dataset using feature thresholds, resulting in a sequence of branching rules and a class label at each terminal node. Its decision process is expressed as explicit if-then rules, which makes the basis for classification easier to review in clinical practice [9]. Decision trees can incorporate both continuous and categorical predictors with minimal preprocessing, and their rule-based structure is consistent with stepwise discrimination reasoning, supporting their use in clinical discrimination modeling [10]. Although machine learning has been increasingly used in tumor imaging assessment [11-13], studies that build an interpretable model combining multimodal breast MRI and axillary ultrasound features specifically for ALNM assessment in BC remain limited. Most existing studies in this area have focused on discrimination performance alone. Few studies have further examined whether noninvasive imaging models may be relevant to surgical planning, adjuvant treatment decisions, or prognostic stratification. As a result, such discrimination models have not been effectively translated into routine clinical practice, and the practical challenges in individualized BC management remain insufficiently addressed.

In this study, we integrated routinely available breast MRI and axillary ultrasound features to construct an interpretable decision tree for preoperative axillary risk stratification in breast cancer. Rather than positioning the model as a substitute for pathological staging, we evaluated whether a rule-based imaging tool could provide clinically understandable risk stratification before surgery. We further explored, in a retrospective manner, the associations of model-defined risk strata with actual axillary surgical management, postoperative morbidity, and short-term outcomes. The purpose of this study was to provide preliminary evidence for the potential clinical utility of imaging-based axillary risk stratification and to inform future prospective validation.

Materials and methods

Study design

This was a single-center retrospective cohort study conducted at Cancer Hospital of Shantou University Medical College. The protocol was approved by the Medical Ethics Committee of Cancer Hospital of Shantou University Medical College and adhered to the principles of the Declaration of Helsinki. Because only anonymized and de-identified retrospective data were used, written informed consent was waived.

Table 1. Patient screening process

Screening process	n
Initially screened women with surgically treated breast cancer between January 2023 and December 2024	394
Excluded cases	190
Bilateral breast cancer, recurrent breast cancer, or concomitant primary malignancy in another system	31
Breast MRI or axillary ultrasound not performed within 2 weeks before surgery, missing sequences, severe artifacts, or insufficient imaging quality	57
Anti-tumor treatment before surgery, including neoadjuvant chemotherapy, endocrine therapy, targeted therapy, or radiotherapy	38
Coexisting axillary conditions potentially affecting nodal imaging assessment, including lymphadenitis, lymphoma, tuberculosis, or other benign nodal diseases	17
Axillary nodal status evaluated only by needle biopsy or incomplete pathological nodal confirmation	22
Incomplete key clinical, imaging, pathological, or follow-up records	25
Final included cohort	204
Pathologically confirmed ALNM	82
No pathologically confirmed ALNM	122

Note: ALNM: Axillary lymph node metastasis; MRI: magnetic resonance imaging.

Study subjects

Patients were screened according to the predefined inclusion and exclusion criteria, and the enrollment process is summarized in **Table 1**. Eligible patients were required to have primary unilateral breast cancer confirmed by postoperative paraffin pathology, preoperative breast MRI and axillary ultrasound performed within 2 weeks before surgery, no anti-tumor treatment before surgery, and complete clinical, imaging, and pathological records. Patients were excluded if they had bilateral or recurrent breast cancer, concomitant malignancies, inadequate imaging quality, axillary diseases that could affect nodal imaging assessment, nodal status evaluated only by needle biopsy, or incomplete key documentation. We retrospectively enrolled 204 female patients with primary BC who underwent surgery in the Department of Breast Surgery of Cancer Hospital of Shantou University Medical College from January 2023 to December 2024. Postoperative paraffin pathology was used as the reference standard to determine axillary nodal status. Patients were assigned to the Metastatic group (n=82) or the Non-metastatic group (n=122). ALNM was defined as tumor infiltration in axillary lymph nodes confirmed on postoperative paraffin pathology, including micrometastases (maximum diameter 0.2-2 mm) and macrometastases (maximum diameter >2 mm). Non-ALNM was defined as negative SLNB on pathology, or no tumor infiltration in any resected axillary lymph node among patients who underwent ALND.

Inclusion criteria

① Primary unilateral BC confirmed by postoperative paraffin pathology; ② Multimodal breast MRI and axillary ultrasound completed in our hospital within 2 weeks before surgery, with imaging quality sufficient for feature assessment and parameter measurement; ③ No anti-tumor treatment before surgery, including neoadjuvant chemotherapy, radiotherapy, endocrine therapy, or targeted therapy; ④ Records complete for clinical, imaging, and pathological variables, with ALNM status clearly documented and no missing key study variables.

Exclusion criteria

① Bilateral BC, recurrent BC, or concomitant primary malignancies in other systems; ② Missing sequences or severe artifacts that prevented imaging assessment or measurement; ③ Coexisting conditions likely to alter axillary lymph node imaging, including axillary lymphadenitis, lymphoma, or tuberculosis; ④ Axillary nodal status evaluated only by needle biopsy (without SLNB/ALND), or incomplete clinical/pathological documentation.

Multimodal breast MRI examination

Multimodal breast MRI was acquired on a 3.0T scanner (Siemens Skyra, Germany) with

an 8-channel dedicated breast phased-array coil. Patients were positioned prone with both breasts naturally suspended in the coil aperture, and scanning commenced after stable positioning. The sequences and parameters were as follows: ① Axial T1-weighted imaging (T1WI): TR 500 ms, TE 8.5 ms, slice thickness 3 mm, slice gap 0.3 mm, FOV 340×340 mm, matrix 320×256; ② Axial fat-suppressed T2-weighted imaging (T2WI-FS): TR 3600 ms, TE 85 ms, slice thickness 3 mm, slice gap 0.3 mm, FOV 340×340 mm, matrix 320×256; ③ Diffusion-weighted imaging (DWI): single-shot echo-planar imaging, TR 4200 ms, TE 72 ms, b values 0 and 800 s/mm^2, slice thickness 4 mm, slice gap 0.4 mm, FOV 320×320 mm, matrix 128×128; ④ Dynamic contrast-enhanced MRI (DCE-MRI): 3D volumetric interpolated breath-hold examination sequence, TR 4.5 ms, TE 2.2 ms, flip angle 10°, slice thickness 1.5 mm, no slice gap, FOV 340×340 mm, matrix 384×384. Gadopentetate dimeglumine was administered via the cubital vein at 0.2 mmol/kg at 2.5 mL/s, followed by a 20 mL saline flush. Dynamic imaging started immediately after injection. Eight consecutive phases were acquired, with a single-phase acquisition time of 60 s.

Axillary ultrasound examination

Axillary ultrasound was performed using a color Doppler ultrasound system (GE Logiq E9, USA) equipped with a 9-15 MHz linear-array transducer, in accordance with the Guidelines for Breast Ultrasound Examination (2022 Edition). Examinations were performed with patients in the supine position and both arms elevated and abducted to facilitate access to the breasts, axillae, and infraclavicular/subclavian regions. After standard assessment of the primary breast lesion, the axilla was systematically scanned in both transverse and longitudinal planes, with evaluation of nodal levels I, II, and III. The scanning range extended from the subclavian region superiorly to the inferior edge of the axillary tail, from the parasternal line medially to the anterior border of the latissimus dorsi laterally.

For each detected axillary lymph node, gray-scale images in long-axis and short-axis planes were recorded, followed by color Doppler flow imaging. Gain and velocity scale were adjusted to display blood-flow signals clearly while minimizing artifacts. Examinations were completed by radiologists with >5 years of experience in breast ultrasound, and images were stored in the PACS.

Standardization of imaging parameter interpretation

Two radiologists with >5 years of experience in breast imaging independently reviewed and measured all imaging data. The readers were blinded to pathological results and clinical information, and to each other's interpretations. Any discrepancies were resolved by joint review until consensus was reached. All imaging examinations were performed preoperatively (within 2 weeks before surgery) and stored in the PACS system before any surgical intervention. The readers were blinded to postoperative pathological results, clinical outcomes, and each other's interpretations, simulating a prospective discrimination scenario. Interobserver agreement was assessed using Cohen's kappa coefficient for categorical variables and intraclass correlation coefficient (ICC) for continuous variables. The kappa values were 0.87 for lymph node hilum integrity, 0.82 for Adler blood flow grade, 0.79 for lymph node microcalcification, 0.76 for lesion margin morphology, and 0.78 for TIC curve type. The ICC was 0.91 for ADC value and 0.89 for RI, indicating good to excellent interobserver agreement.

Interpretation indicators of multimodal breast MRI: ① Quantitative indicator: apparent diffusion coefficient (ADC) value (the region of interest was placed in the solid component of the lesion on DWI, avoiding cystic change, necrosis, and hemorrhage; measurements were repeated three times and averaged); ② Qualitative indicators: time-signal intensity curve (TIC) type (type I: persistent enhancement, type II: plateau, type III: washout), lesion margin (smooth, lobulated, spiculated), enhancement pattern (homogeneous, heterogeneous, rim enhancement), nipple involvement, and chest wall invasion.

Interpretation indicators of axillary ultrasound: ① Quantitative indicator: resistance index (RI); ② Qualitative indicators: hilum integrity (pres-

ent, partially absent, completely absent), internal echogenicity (homogeneous, heterogeneous), microcalcification (present, absent), and Adler blood flow grade (grade 0: no flow signal; grade I: minimal flow, 1-2 punctate signals; grade II: moderate flow, 3-4 punctate signals or 1 clear vessel; grade III: abundant flow, ≥5 punctate signals or ≥2 clear vessels).

Observation indicators

① Baseline clinicopathological characteristics were compared between the Metastatic group and Non-metastatic group, including age, menopausal status, BMI, tumor location, pathological type, histological grade, ER, PR, HER2, Ki-67, and molecular subtype; ② Quantitative and qualitative parameters of multimodal breast MRI were compared between the two groups; ③ Quantitative and qualitative parameters of axillary ultrasound were compared between the two groups; ④ Associations between imaging parameters and ALNM were analyzed; ⑤ A decision tree model was constructed and evaluated based on imaging variables; ⑥ Internal validation of the decision tree model was performed; ⑦ Retrospective indicators related to axillary management patterns: these included the actual axillary procedure performed (omission of sentinel lymph node biopsy [SLNB], SLNB alone, or axillary lymph node dissection [ALND]). To describe the potential mismatch between pathological nodal status and the extent of axillary intervention in each model-defined risk stratum, we calculated the proportion of pathologically node-negative patients who nevertheless underwent SLNB/ALND and the proportion of patients with pathologically confirmed macrometastasis who did not undergo ALND; ⑧ Postoperative safety indicators: complications related to axillary surgery within 1 year after surgery were recorded, including upper-extremity lymphedema, sensory disturbance, incision infection, subcutaneous seroma, restricted shoulder mobility, and the overall complication rate; ⑨ Short-term survival outcome indicators: 1-year disease-free survival (DFS) after surgery was used as the primary endpoint and was defined as the time from the date of surgery to the first occurrence of local recurrence, distant metastasis, or all-cause death; for patients without endpoint events, the date of the last follow-up was taken as the censoring time. At the same time, exploratory associations between postoperative adjuvant therapy, including chemotherapy, radiotherapy, endocrine therapy, and targeted therapy, and 1-year DFS were described across different risk strata.

Statistical analysis

Statistical analyses were conducted using SPSS 26.0 and R 4.3.1. Two-sided $P<0.05$ was considered statistically significant. Continuous variables with normal distribution are presented as mean ± standard deviation and were compared using the independent-samples t test (two groups) or one-way analysis of variance (multiple groups), with the LSD-t test used for post hoc pairwise comparisons. Categorical variables are presented as n (%) and were compared using the chi-square test; Fisher's exact test was applied when the expected frequency was <5.

ALNM status served as the outcome variable. MRI- and ultrasound-derived parameters were considered candidate predictors. Variables significant in univariate analyses ($P<0.05$) were entered into an unconditional multivariable logistic regression model. Forward stepwise selection using the likelihood-ratio test was applied to retain independent predictors; effect estimates are reported as odds ratios (ORs) with 95% confidence intervals (CIs). We built a CART decision tree using the Gini impurity as the split criterion. ROC analysis was used to evaluate model discrimination, and we reported the AUC, sensitivity, and specificity. For internal validation, we used a 7:3 random split, with 70% of patients going to the training set and 30% going to the validation set. This random split was used as an exploratory internal validation approach rather than as definitive evidence of model generalizability. Given the retrospective single-center design and moderate sample size, the validation results were interpreted conservatively and were not used to claim clinical readiness of the model. To reduce selection bias, all patients were enrolled in the study period. Because the model was derived from preoperative imaging findings and verified against postoperative pathology, its role in this study was limited to preoperative risk stratification rather than replacement of pathological confirmation.

Table 2. Baseline data of BC patients in metastatic group and non-metastatic group

Indicator	Metastatic group (n=82)	Non-metastatic group (n=122)	t/χ^2	P
Age (years)	51.68±8.64	50.54±9.32	0.866	0.388
Menopausal status			1.063	0.303
Premenopausal	39 (47.56)	67 (54.92)		
Postmenopausal	43 (52.44)	55 (45.08)		
BMI (kg/m^2, mean ± SD)	22.26±3.26	23.02±3.15	1.64	0.103
Tumor location			0.107	0.744
Left breast	45 (54.88)	64 (52.46)		
Right breast	37 (45.12)	58 (47.54)		
Tumor quadrant			0.517	0.972
Upper outer quadrant	48 (58.54)	69 (56.56)		
Upper inner quadrant	14 (17.07)	23 (18.85)		
Lower outer quadrant	11 (13.41)	18 (14.75)		
Lower inner quadrant	5 (6.10)	8 (6.56)		
Central region	4 (4.88)	4 (3.28)		
Pathological type			0.959	0.619
Invasive ductal carcinoma	76 (92.68)	108 (88.52)		
Invasive lobular carcinoma	3 (3.66)	7 (5.74)		
Other special types of carcinoma	3 (3.66)	7 (5.74)		
Histological grade			13	0.002
Grade I	8 (9.76)	27 (22.13)		
Grade II	36 (43.90)	66 (54.10)		
Grade III	38 (46.34)	29 (23.77)		
ER expression status			5.263	0.022
Positive	51 (62.20)	94 (77.05)		
Negative	31 (37.80)	28 (22.95)		
PR expression status			5.394	0.02
Positive	47 (57.32)	89 (72.95)		
Negative	35 (42.68)	33 (27.05)		
HER2 expression status			6.103	0.014
Positive	32 (39.02)	28 (22.95)		
Negative	50 (60.98)	94 (77.05)		
Ki-67 proliferation index			8.825	0.003
Low expression (<20%)	22 (26.83)	58 (47.54)		
High expression (≥20%)	60 (73.17)	64 (52.46)		

Note: BC: Breast cancer; BMI: body mass index; SD: standard deviation; ER: estrogen receptor; PR: progesterone receptor; HER2: human epidermal growth factor receptor 2; Ki-67: Ki-67 proliferation index.

Kaplan-Meier analysis was used to estimate the 1-year DFS rate and its 95% confidence interval, and survival differences between groups were compared with the log-rank test. A multivariate Cox proportional hazards regression model was then applied to evaluate the effect of postoperative adjuvant therapy on DFS after adjustment for confounding factors such as age, tumor T stage, and molecular subtype. Hazard ratios (HRs) and 95% confidence intervals were calculated, and interaction analysis was further performed to clarify the relationship between model-based risk stratification and exploratory short-term DFS findings.

Results

Baseline characteristics of study subjects

The two groups were comparable in age, menopausal status, BMI, tumor location, tumor quadrant, and pathological type (all P>0.05) (**Table 2**). Significant between-group differenc-

Table 3. Comparison of Multimodal breast MRI parameters of patients in the two groups

Indicator	Metastatic group (n=82)	Non-metastatic group (n=122)	t/χ^2	P
ADC value ($\times 10^{-3}$ mm^2/s)	1.04±0.30	1.14±0.26	2.559	0.011
TIC curve type			6.811	0.009
Type I (persistent ascending)	24 (29.27)	58 (47.54)		
Type II+ III (platform + washout)	58 (70.73)	64 (52.46)		
Lesion margin morphology			9.05	0.003
Smooth/lobulated	51 (62.20)	99 (81.15)		
Spiculated	31 (37.80)	23 (18.85)		
Lesion enhancement homogeneity			1.478	0.224
Homogeneous enhancement	28 (34.15)	52 (42.62)		
Heterogeneous/ring enhancement	54 (65.85)	70 (57.38)		
Nipple involvement			2.874	0.09
Absent	69 (84.15)	112 (91.80)		
Present	13 (15.85)	10 (8.20)		
Chest wall invasion			-	0.064*
Absent	79 (96.34)	122 (100.00)		
Present	3 (3.66)	0 (0.00)		

*Note: Fisher's exact test was used for chest wall invasion due to theoretical frequency <5. MRI: Magnetic resonance imaging; ADC: apparent diffusion coefficient; TIC: time-signal intensity curve.

es were observed for histological grade and ER, PR, HER2, and Ki-67 status (P<0.05) (**Table 2**).

Comparison of multimodal breast MRI parameters between the two groups

Lesion enhancement homogeneity, nipple involvement, and chest wall invasion did not differ between groups (all P>0.05) (**Table 3**). The Metastatic group showed lower ADC values than the Non-metastatic group (P=0.011). TIC type distribution differed significantly (P=0.009), with a higher proportion of type II/III patterns in the Metastatic group (**Table 3**). Lesion margin morphology also differed (P=0.003), and spiculated margins were more frequently observed in the Metastatic group (**Table 3**).

Comparison of axillary ultrasound parameters between the two groups

Internal echo homogeneity was similar between groups (P>0.05). RI was higher in the Metastatic group (P<0.001). Compared with the Non-metastatic group, the Metastatic group had lower proportions of intact lymph node hilum (P<0.001), absence of microcalcification (P=0.001), and Adler grade 0-I (P<0.001) (**Table 4**).

Multivariate analysis of factors associated with ALNM

Multivariate logistic regression was conducted with ALNM as the dependent variable and imaging variables significant in univariate comparisons as covariates (**Table 5**). ADC (P=0.122) and TIC type (P=0.057) were not retained as independent factors. Lesion margin morphology (OR=2.511, 95% CI=1.141-5.529), RI (OR=5.040, 95% CI=1.080-23.256), lymph node hilum integrity (OR=6.904, 95% CI=3.004-15.867), lymph node microcalcification (OR=3.900, 95% CI=1.194-12.736), and Adler blood flow grade (OR=4.837, 95% CI=2.340-10.000) were independently associated with ALNM (P<0.05) (**Table 6**).

Development of the imaging-based decision tree for preoperative axillary risk stratification

A CART decision tree was built using the imaging factors identified in multivariate analysis. The model was trained with a maximum depth of 5, a minimum parent-node size of 10, and a minimum leaf-node size of 5. In the final tree, lymph node hilum integrity was the primary split variable and the highest-ranked feature, followed by Adler blood flow grade, lesion margin morphology, lymph node microcalcification,

Table 4. Axillary ultrasound parameters of patients in the two groups

Indicator	Metastatic group (n=82)	Non-metastatic group (n=122)	t/χ^2	P
RI	0.77±0.22	0.63±0.27	3.946	<0.001
Lymph node hilum structure integrity			31.482	<0.001
Present	45 (54.88)	109 (89.34)		
Partially/completely disappeared	37 (45.12)	13 (10.66)		
Internal echo homogeneity			3.595	0.058
Homogeneous	54 (65.85)	95 (77.87)		
Heterogeneous	28 (34.15)	27 (22.13)		
Lymph node microcalcification			10.864	0.001
Absent	66 (80.49)	116 (95.08)		
Present	16 (19.51)	6 (4.92)		
Adler blood flow grade			25.053	<0.001
Grade 0-I	28 (34.15)	85 (69.67)		
Grade II-III	54 (65.85)	37 (30.33)		

Note: RI: Resistance index.

Table 5. Variable assignment table

Variable type	Variable name	Assignment method
Dependent variable	ALNM	Absent =0, Present =1
Covariate	ADC value, RI	Original data included in the analysis
	TIC curve type	Type I =0, Type II + III =1
	Lesion margin morphology	Smooth/lobulated =0, Spiculated =1
	Lymph node hilum structure integrity	Present =0, Partially/completely disappeared =1
	Lymph node microcalcification	Absent =0, Present =1
	Adler blood flow grade	Grade 0-I =0, Grade II-III =1

Note: ALNM: Axillary lymph node metastasis; ADC: apparent diffusion coefficient; RI: resistance index; TIC: time-signal intensity curve.

Table 6. Multivariate Logistic regression analysis results of ALNM in BC patients

Variable	B value	S.E.	Wald χ^2 value	P	OR	95% CI	
ADC value	1.065	0.689	2.388	0.122	2.9	0.752	11.192
TIC curve type	0.725	0.38	3.636	0.057	2.066	0.98	4.354
Lesion margin morphology	0.921	0.403	5.231	0.022	2.511	1.141	5.529
RI	1.617	0.786	4.235	0.040	5.040	1.080	23.256
Lymph node hilum structure integrity	1.932	0.425	20.71	<0.001	6.904	3.004	15.867
Lymph node microcalcification	1.361	0.604	5.081	0.024	3.9	1.194	12.736
Adler blood flow grade	1.576	0.371	18.102	<0.001	4.837	2.34	10

Note: ALNM: Axillary lymph node metastasis; BC: breast cancer; S.E.: standard error; OR: odds ratio; CI: confidence interval; ADC: apparent diffusion coefficient; TIC: time-signal intensity curve; RI: resistance index.

and RI (**Figure 1**). To improve clinical readability, the CART structure was also summarized as a simplified stepwise clinical decision pathway based on the same imaging variables (**Table 7**). This pathway was intended to help clinicians understand the sequence of imaging assessment and does not replace the original model or pathological confirmation.

Discriminative performance of the decision tree in axillary risk stratification

ROC analysis showed moderate discrimination of the decision tree for preoperative axillary risk stratification, with a sensitivity of 69.51%, a specificity of 84.43%, and an AUC of 0.829 (95% CI=0.770-0.883; P<0.001) (**Figure 2**).

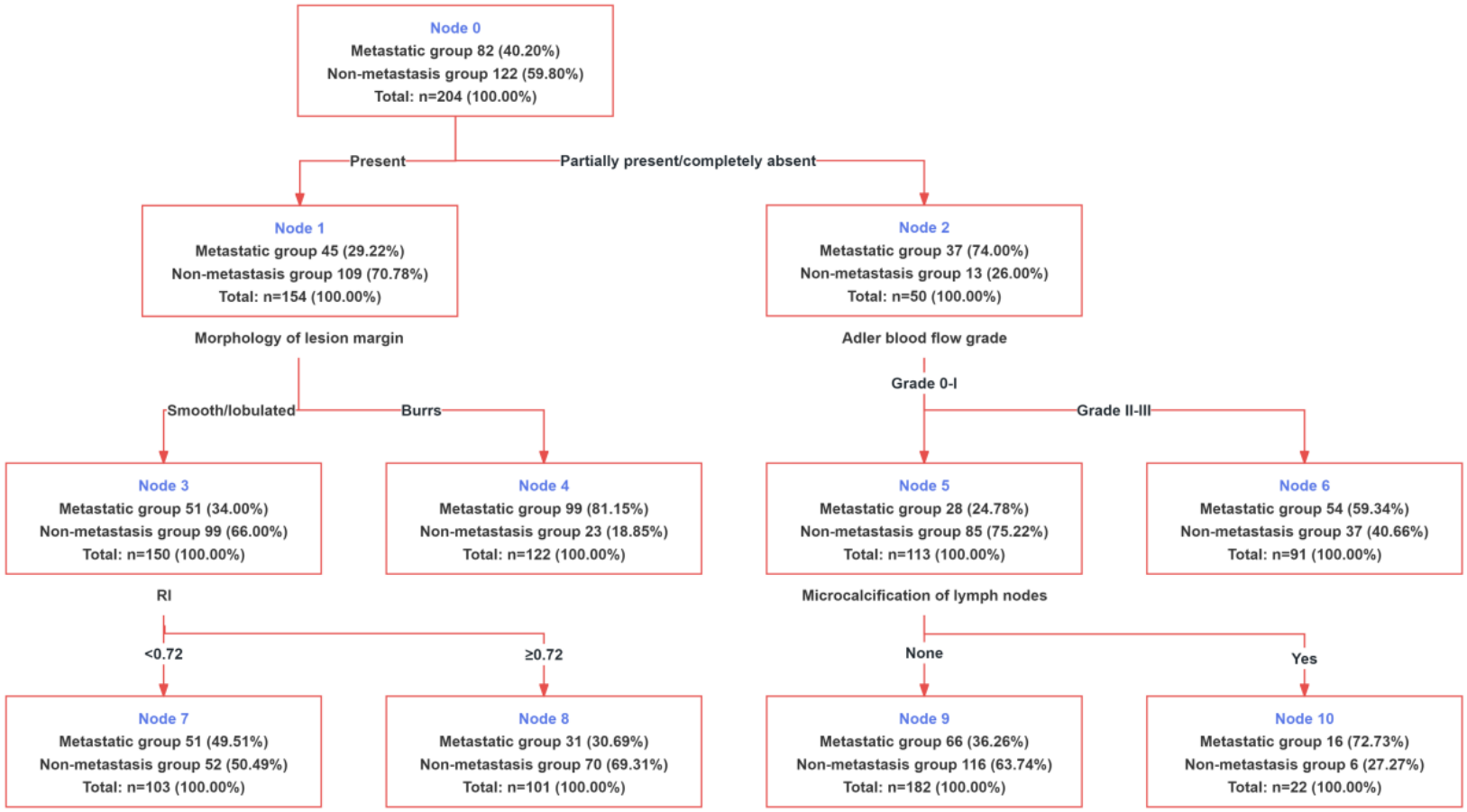

Figure 1. CART decision tree for preoperative axillary risk stratification in breast cancer. A simplified clinical interpretation of the CART pathway is provided in **Table 7** to improve readability for clinical users. CART: Classification and regression tree; RI: resistance index.

Table 7. Simplified clinical decision pathway derived from the CART model

Step	Imaging feature	Practical interpretation	Suggested clinical use
Step 1	Lymph node hilum integrity on axillary ultrasound	Preserved hilum generally indicates lower nodal suspicion, whereas partial or complete hilum loss increases suspicion of ALNM.	Use as the first-line imaging feature for preoperative axillary risk assessment.
Step 2	Adler blood flow grade	Grade 0-I supports lower vascular suspicion; grade II-III suggests increased nodal vascularity and higher metastatic probability.	Use to further stratify patients when nodal morphology is abnormal or equivocal.
Step 3	Lesion margin morphology on breast MRI	Smooth or lobulated margins support lower risk; spiculated margins suggest more aggressive tumor behavior and higher ALNM probability.	Incorporate primary-tumor morphology when axillary findings alone are insufficient for risk judgment.
Step 4	Lymph node microcalcification	Absence of microcalcification supports lower suspicion; presence of microcalcification increases suspicion of metastatic involvement.	Use as an additional risk-escalating feature in the stepwise assessment.
Step 5	Ultrasound RI	A lower RI supports lower vascular resistance, whereas a higher RI supports increased suspicion of metastatic involvement.	Use as a quantitative modifier when final risk stratification remains uncertain.
Final interpretation	Integration of CART-derived imaging features	Patients are categorized into low-, intermediate-, or high-risk groups according to the CART pathway.	This pathway may assist preoperative risk communication and multidisciplinary discussion, but it should not replace SLNB, ALND, or pathological confirmation.

Note: CART: Classification and regression tree; ALNM: axillary lymph node metastasis; MRI: magnetic resonance imaging; RI: resistance index; SLNB: sentinel lymph node biopsy; ALND: axillary lymph node dissection.

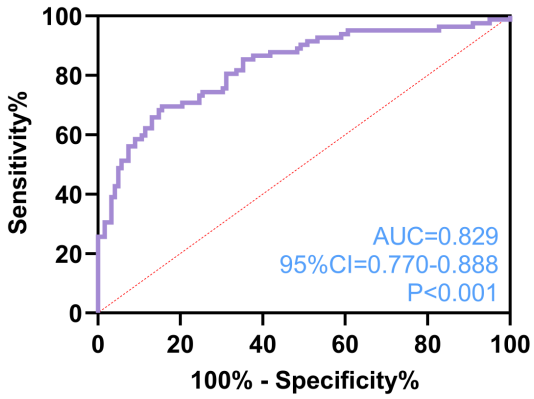

Figure 2. ROC curve of the CART decision tree for axillary risk stratification in the overall cohort. ROC: Receiver operating characteristic; CART: classification and regression tree; AUC: area under the curve; CI: confidence interval.

Internal validation of the decision tree model

For internal validation, the cohort was randomly divided into a training set (n=143) and a validation set (n=61) at a 7:3 ratio. In the training set, sensitivity was 73.33% and specificity was 83.13% (AUC=0.835, 95% CI=0.767-0.903). In the validation set, sensitivity was 81.82% and specificity was 74.36% (AUC=0.803, 95% CI=0.678-0.928) (**Figure 3**). Baseline clinicopathological and imaging characteristics were generally comparable between the two sets. However, because this validation was based on a single random split, the result should be interpreted as preliminary internal evidence rather than proof of stable performance across different samples or institutions.

Distribution of axillary surgical strategies and rates of potentially avoidable invasive axillary intervention/undertreatment across different model-based risk strata

Among patients classified into low-, intermediate-, and high-risk groups by the decision tree, the observed rate of pathologically confirmed ALNM increased stepwise across strata. The actual distribution of axillary surgical procedures also differed significantly among the three groups (χ^2=42.185, P<0.001). Importantly, all surgical decisions in this cohort were made on the basis of routine clinical judgment rather than model output. In retrospective analyses, SLNB omission was observed only in the low-risk group. Among pathologically node-negative patients, the proportion undergoing invasive axillary staging or dissection remained high across strata. By contrast, the proportion of patients with macrometastatic disease who did not undergo ALND did not differ significantly between groups (χ^2=0.217, P=0.897) (**Table 8**).

Comparison of key perioperative indicators among patients undergoing different axillary surgical strategies

In the ALND group, operative time was longer, intraoperative blood loss was greater, and drainage tube duration was prolonged compared with both the SLNB-only group and the SLNB-omission group. These same perioperative indicators were also higher in the SLNB-only group than in the SLNB-omission group (all P<0.05). In addition, the incidence of delayed postoperative wound healing differed significantly among the three groups (P<0.001), and this complication occurred more frequently in the ALND group than in the other two groups (**Table 9**).

Postoperative safety in patients undergoing different axillary surgical procedures

The 1-year follow-up results showed that no postoperative complications occurred in the group exempted from SLNB, whereas the overall complication rate was 25.81% in the SLNB-only group and increased to 79.41% in the ALND group. Stratified analysis of individual complications showed significant differences among the three groups in the incidence of upper-extremity lymphedema (χ^2=25.361, P<0.001), upper-extremity sensory disturbance (χ^2=33.105, P<0.001), subcutaneous seroma (χ^2=15.026, P<0.001), and restricted shoulder mobility (χ^2=21.485, P<0.001) (**Table 10**).

Comparison of upper limb function scores at 1 year after surgery among patients undergoing different axillary surgical strategies

Evaluation of upper limb function at 1 year after surgery showed significant differences among the three groups in both the total DASH score and all dimensional scores (P<0.001). The SLNB-omission group had the lowest DASH scores, indicating the best preservation of

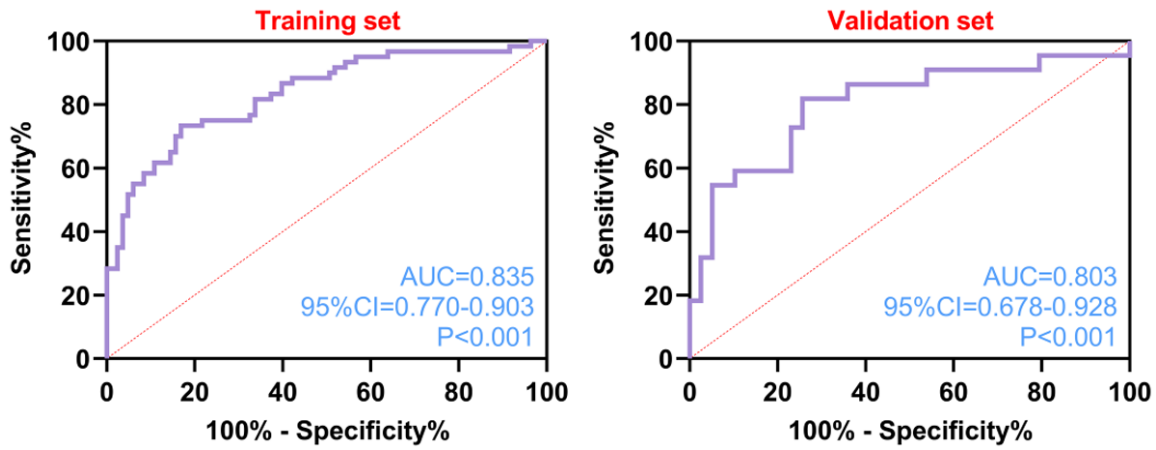

Figure 3. ROC curves of the CART decision tree model in the training set and validation set for internal validation. ROC: Receiver operating characteristic; CART: classification and regression tree; AUC: area under the curve; CI: confidence interval.

upper limb function. In contrast, patients who underwent ALND showed significantly higher total and dimensional scores than those in the SLNB-only group and the SLNB-omission group, while the SLNB-only group also scored significantly higher than the SLNB-omission group (P<0.001). Overall, greater axillary surgical extent was associated with worse postoperative upper-limb function (**Table 11**).

Comparison of treatment burden indicators within 1 year after surgery among patients undergoing different axillary surgical strategies

The three groups also differed significantly in total postoperative length of hospitalization, total inpatient medical costs, and the number of rehabilitation follow-up visits within 1 year after surgery (all P<0.001). Specifically, patients in the ALND group had longer postoperative hospital stays, incurred higher medical costs, and required more rehabilitation visits than those in the SLNB-only group and the SLNB-omission group. The same trend was observed when the SLNB-only group was compared with the SLNB-omission group, with all three indicators remaining significantly higher in the former group (all P<0.05) (**Table 12**).

Distribution of postoperative regional radiotherapy decisions among patients undergoing different axillary surgical strategies

No patients in the SLNB-omission group received any postoperative regional radiotherapy. In the SLNB-only group, treatment was mainly limited to no radiotherapy or whole-breast irradiation alone, and the proportion receiving regional nodal irradiation was only 4.03%. By comparison, 64.71% of patients in the ALND group underwent regional nodal irradiation, a rate that was significantly higher than that in both the SLNB-omission group and the SLNB-only group (P<0.001) (**Table 13**).

Hypothesis-generating descriptive analysis of 1-year DFS after postoperative adjuvant therapy across model-defined risk strata

As a hypothesis-generating descriptive analysis, we explored whether the association between postoperative adjuvant therapy and 1-year DFS differed across model-defined risk strata. After adjustment for age, tumor T stage, molecular subtype, and other confounders, no statistically significant association between adjuvant therapy and 1-year DFS was observed in the low-risk group. In the intermediate- and high-risk groups, the hazard ratios were numerically below 1.0, but the confidence intervals were wide and crossed 1.0. In particular, only two high-risk patients did not receive postoperative adjuvant therapy, resulting in highly unstable estimates. Therefore, these findings should be interpreted as descriptive and hypothesis-generating only and should not be used to infer treatment benefit, treatment selection, or treatment de-escalation (**Table 14**).

Table 8. Distribution of axillary surgical strategies and retrospective mismatch rates between pathological nodal status and extent of axillary intervention across model-defined risk strata

		Low-risk Group (n=102)	Medium-risk Group (n=58)	High-risk Group (n=44)	Total	χ^2	P
Pathological No Metastasis		94 (92.16)	22 (37.93)	6 (13.64)	122 (59.80)	-	
Pathological Metastasis		8 (7.84)	36 (62.07)	38 (86.36)	82 (40.20)	-	
Actual axillary surgery plan	SLNB (Sentinel Lymph Node Biopsy) Exempted	12 (11.76)	0 (0.00)	0 (0.00)	12 (5.88)	42.185	<0.001
	SLNB (Sentinel Lymph Node Biopsy) Only	78 (76.47)	41 (70.69)	5 (11.36)	124 (60.78)		
	ALND (Axillary Lymph Node Dissection) Performed	12 (11.77)	17 (29.31)	39 (88.64)	68 (33.33)		
Over-treatment Rate		78 (82.98)	15 (68.18)	5 (83.33)	-	21.364	<0.001
Under-treatment Rate		1 (12.50)	2 (5.56)	3 (7.89)	-	0.217	0.897

Note: potentially avoidable invasive axillary intervention rate was calculated as (number of pathologically node-negative patients who underwent SLNB/ALND)/(total number of pathologically node-negative patients in the corresponding risk stratum) × 100%. Undertreatment rate was calculated as (number of patients with pathologically confirmed macrometastasis who did not undergo standard ALND)/(total number of patients with pathologically confirmed macrometastasis in the corresponding risk stratum) × 100%. SLNB: Sentinel lymph node biopsy; ALND: axillary lymph node dissection.

Table 9. Comparison of key perioperative indicators among patients undergoing different axillary surgical strategies

Groups	n	Operation time (min)	Intraoperative blood loss (mL)	Postoperative drainage tube indwelling time (d)	Postoperative incision healing was delayed
SLNB (Sentinel Lymph Node Biopsy) Exempted	12	55.17±12.45	15.25±4.35	-	0 (0.00)
SLNB (Sentinel Lymph Node Biopsy) Only	124	74.43±14.64*	27.59±10.36*	3.94±1.00	4 (3.23)
ALND (Axillary Lymph Node Dissection) Performed	68	121.04±20.33*,#	43.10±15.23*,#	6.47±2.02	11 (16.18)*,#
Statistics		F=198.138	F=49.151	t=11.612	χ^2=11.823
P		<0.001	<0.001	<0.001	<0.001

Note: * indicates P<0.05 compared with SLNB (Sentinel Lymph Node Biopsy) Exempted, # indicates P<0.05 compared with SLNB (Sentinel Lymph Node Biopsy) Only. SLNB: Sentinel lymph node biopsy; ALND: axillary lymph node dissection.

Table 10. One-year postoperative complication rates in patients undergoing different axillary surgical procedures

Groups	n	Upper Extremity Lymphedema	Upper Extremity Paresthesia	Incision Infection	Subcutaneous Effusion	Shoulder Joint Mobility Limitation	Total Complication Rate
SLNB (Sentinel Lymph Node Biopsy) Exempted	12	0 (0.00)	0 (0.00)	0 (0.00)	0 (0.00)	0 (0.00)	0 (0.00)
SLNB (Sentinel Lymph Node Biopsy) Only	124	8 (6.45)	14 (11.29)*	3 (2.42)	9 (7.26)	3 (2.42)	32 (25.81)*
ALND (Axillary Lymph Node Dissection) Performed	68	16 (23.53)*,#	21 (30.88)*,#	6 (8.82)*,#	14 (20.59)*,#	11 (16.18)*,#	54 (79.41)*,#
χ^2		25.361	33.105	0.118	15.026	21.485	65.294
P		<0.001	<0.001	0.118	<0.001	<0.001	<0.001

Note: * indicates P<0.05 compared with SLNB (Sentinel Lymph Node Biopsy) Exempted, # indicates P<0.05 compared with SLNB (Sentinel Lymph Node Biopsy) Only. SLNB: Sentinel lymph node biopsy; ALND: axillary lymph node dissection.

Table 11. Comparison of upper limb function scores at 1 year after surgery among patients undergoing different axillary surgical strategies

Groups	n	The DASH upper limb function score	Daily activity ability dimension	Motor function dimension	Symptom related dimensions
SLNB (Sentinel Lymph Node Biopsy) Exempted	12	6.83±2.52	4.17±0.94	4.50±2.02	4.25±1.71
SLNB (Sentinel Lymph Node Biopsy) Only	124	18.74±4.01*	15.88±5.88*	16.56±5.64*	15.79±5.96*
ALND (Axillary Lymph Node Dissection) Performed	68	31.25±14.81*,#	32.97±12.56*,#	44.18±9.98*,#	37.16±10.28*,#
F		59.314	111.104	367.522	211.806
P		<0.001	<0.001	<0.001	<0.001

Note: * indicates P<0.05 compared with SLNB (Sentinel Lymph Node Biopsy) Exempted, # indicates P<0.05 compared with SLNB (Sentinel Lymph Node Biopsy) Only. SLNB: Sentinel lymph node biopsy; ALND: axillary lymph node dissection; DASH: Disabilities of the Arm, Shoulder and Hand.

Table 12. Comparison of treatment burden indicators within 1 year after surgery among patients undergoing different axillary surgical strategies

Groups	n	Postoperative hospital stay (d)	Inpatient medical expenses (ten thousand yuan)	Number of rehabilitation visits one year after surgery
SLNB (Sentinel Lymph Node Biopsy) Exempted	12	3.83±1.19	2.13±0.21	2.08±0.67
SLNB (Sentinel Lymph Node Biopsy) Only	124	5.48±1.08*	2.91±0.44	4.03±1.50*
ALND (Axillary Lymph Node Dissection) Performed	68	7.96±1.98*,#	4.31±0.80*,#	5.62±2.04*,#
F		81.527	156.307	32.534
P		<0.001	<0.001	<0.001

Note: * indicates P<0.05 compared with SLNB (Sentinel Lymph Node Biopsy) Exempted, # indicates P<0.05 compared with SLNB (Sentinel Lymph Node Biopsy) Only. SLNB: Sentinel lymph node biopsy; ALND: axillary lymph node dissection.

Table 13. Distribution of postoperative regional radiotherapy decisions among patients undergoing different axillary surgical strategies

Groups	n	No regional radiotherapy was received	Radiotherapy for the entire breast only	Whole breast plus axillary/ supraclavicular radiotherapy
SLNB (Sentinel Lymph Node Biopsy) Exempted	12	12 (100.00%)	0 (0.00%)	0 (0.00%)
SLNB (Sentinel Lymph Node Biopsy) Only	124	97 (78.23%)	22 (17.74%)*	5 (4.03%)
ALND (Axillary Lymph Node Dissection) Performed	68	16 (23.53%)*,#	8 (11.76%)*,#	44 (64.71%)*,#
Total (n=204)		125 (61.27%)	30 (14.71%)	49 (24.02%)
χ^2		63.431	3.449	92.623
P		<0.001	0.178	<0.001

Note: * indicates P<0.05 compared with SLNB (Sentinel Lymph Node Biopsy) Exempted, # indicates P<0.05 compared with SLNB (Sentinel Lymph Node Biopsy) Only. SLNB: Sentinel lymph node biopsy; ALND: axillary lymph node dissection.

Table 14. Hypothesis-generating descriptive analysis of 1-year DFS after postoperative adjuvant therapy across model-defined risk strata

Model Risk Stratification	n	Received Postoperative Adjuvant Therapy		Non-received Postoperative Adjuvant Therapy		HR Value (95% CI)	Interaction *P* Value
		n	1-year DFS (Disease-Free Survival) Rate (95% CI)	n	1-year DFS (Disease-Free Survival) Rate (95% CI)		
Low-risk Group	102	76	98.7% (96.0%-100.0%)	26	96.2% (88.9%-100.0%)	0.785 (0.081-7.624)	0.832
Medium-risk Group	58	49	91.8% (84.4%-99.2%)	9	77.8% (50.7%-100.0%)	0.426 (0.090-2.019)	0.281
High-risk Group	44	42	78.6% (66.7%-90.5%)	2	50.0% (0.0%-100.0%)	0.298 (0.032-2.779)	0.280
Total Cohort	204	167	92.2% (88.3%-96.1%)	37	91.9% (83.2%-100.0%)	0.657 (0.237-1.821)	0.420

Note: DFS: Disease-free survival; HR: hazard ratio; CI: confidence interval. This analysis was exploratory and hypothesis-generating only. Several subgroups contained very small numbers of patients, particularly the high-risk group without postoperative adjuvant therapy. Therefore, the HR estimates and confidence intervals are statistically unstable and should not be used to infer treatment benefit or guide treatment de-escalation.

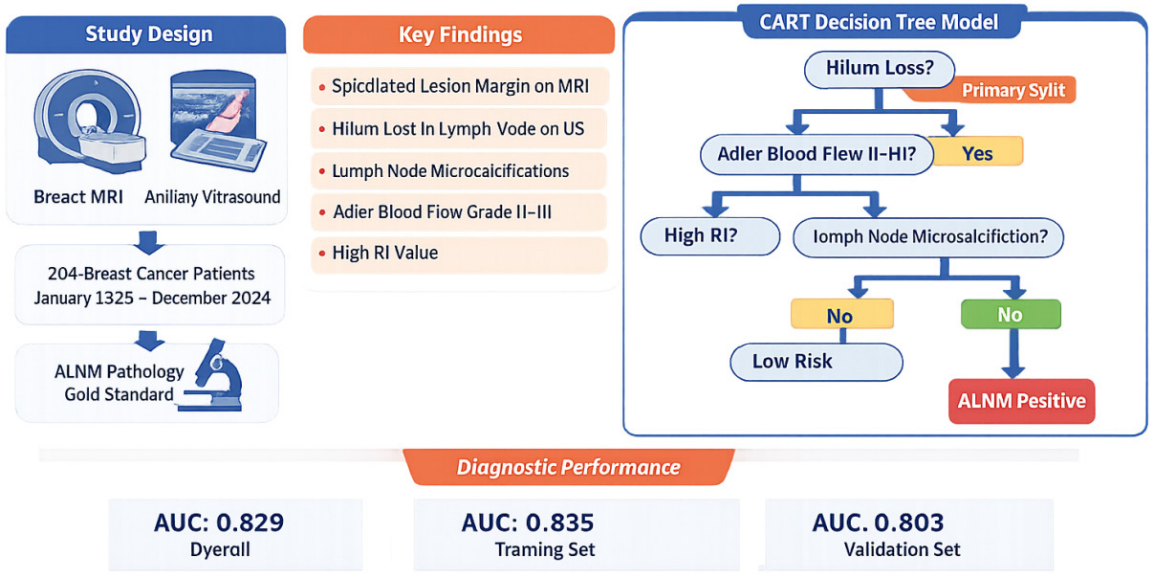

Figure 4. Graphical overview of the study design, key imaging features, and retrospective clinical utility analysis of the multimodal imaging-based decision tree. ALNM: Axillary lymph node metastasis; MRI: magnetic resonance imaging; US: ultrasound; CART: classification and regression tree; RI: resistance index; AUC: area under the curve.

Discussion

We integrated routinely assessed preoperative breast MRI and axillary ultrasound features to construct an interpretable decision tree and examined its potential clinical utility as a tool for preoperative axillary risk stratification in breast cancer. The model provides explicit rule-based outputs that are readily understandable in routine imaging review (**Figure 4**). Rather than testing the model as a tool that directly guided treatment in this cohort, we retrospectively evaluated whether model-defined risk strata were associated with observed axillary management patterns and short-term postoperative outcomes. These findings are intended to provide preliminary clinical context for future prospective validation rather than direct evidence of management benefit.

Multivariate analysis identified lymph node hilum integrity, Adler blood flow grade, MRI lesion margin morphology, lymph node microcalcification, and ultrasound RI as independent variables associated with ALNM, in line with previous reports [14-16]. Lymph node hilum integrity showed the strongest contribution and served as the primary split node in the decision tree. Partial or complete loss of the fatty hilum reflects disruption of nodal architecture by metastatic infiltration and has been regarded as a relatively specific ultrasound feature of nodal metastasis [17, 18]. The present findings support its value as a first-line imaging marker within a stepwise assessment pathway.

Adler blood flow grade and RI, which reflect nodal vascularity and resistance, were also independently associated with ALNM. This finding is consistent with tumor-driven angiogenesis and vascular remodeling in metastatic nodes, where irregular neovessels and increased vascular resistance may manifest as higher vascularity grades and elevated RI [19-21]. Doppler-derived indices have often been treated as ancillary findings in prior work [22, 23]. In our decision tree, both Adler blood flow grade and RI were included as split variables, supporting their clinical utility for sequential stratification. The slight difference in feature ranking can be attributed to their distinct clinical decision-making logics: logistic regression assesses independent statistical effects, whereas a decision tree prioritizes features that offer the clearest and most actionable clinical thresholds. Adler blood flow grade showed more intuitive clinical discriminative power in our cohort, so it was selected as an earlier split.

For primary-tumor MRI, lesion margin morphology remained independently associated with ALNM, with spiculated margins corresponding to a higher likelihood of metastatic involvement. Spiculation is typically linked to infiltrative growth and stromal reaction and may be associated with more aggressive tumor biology. Incorporating primary-lesion morphology into nodal risk estimation is reasonable, particularly when axillary findings are equivocal.

In routine preoperative evaluation, ALNM assessment still depends largely on single-modality interpretation or regression-based risk stratification models [24-26]. Conventional axillary ultrasound may be less sensitive for micrometastases and for deep or atypically located nodes [27], whereas MRI assessment can be confounded by reactive or inflammatory nodal changes that increase false-positive calls [28]. In practice, MRI and ultrasound are frequently interpreted together, but this integration is commonly heuristic and standardized quantitative fusion remains uncommon [29]. Logistic regression yields an estimated probability; however, this output does not always map onto the stepwise decision-making used in clinical image interpretation, which can limit implementation.

Recent studies have increasingly used radiomics, deep learning, multimodal data integration, and SHAP-based interpretability methods for preoperative ALNM prediction [30-33]. These approaches can extract high-dimensional image features and may achieve favorable discrimination in selected cohorts. However, the clinical purpose of the present study was different. We did not aim to maximize predictive performance using raw-image feature extraction. Instead, we sought to transform routinely reported breast MRI and axillary ultrasound findings into a transparent preoperative risk-stratification pathway. The rationale for selecting CART was therefore not interpretability alone. More importantly, the if-then structure of a decision tree closely resembles the stepwise reasoning process used by clinicians during axillary imaging assessment. In the present model, lymph node hilum integrity is evaluated first, followed by Adler blood flow grade, MRI lesion margin morphology, lymph node microcalcification, and RI when further stratification is needed. Each risk assignment can therefore be traced back to specific imaging findings. This structure makes the model easier to review in multidisciplinary discussion and easier to translate into a clinical pathway than black-box models or models requiring post hoc explanation. Thus, the value of this CART model lies in its transparency, low complexity, and compatibility with routine clinical workflow rather than in claiming superiority over deep learning models.

SLNB remains the reference standard for axillary staging, but it is invasive and can be followed by complications such as upper-limb lymphedema, sensory disturbance, and restricted shoulder mobility. Many patients undergoing SLNB are ultimately node-negative and therefore receive an invasive procedure without pathological benefit [34, 35]. Because the model uses preoperative MRI and ultrasound parameters obtained during routine care, it enables non-invasive ALNM risk stratification without additional examinations. External validation is required to determine whether the model can support individualized axillary management and preoperative planning in broader clinical settings. A prospective multicenter validation study is planned in three steps. First, the imaging acquisition protocol, feature definitions, reader training materials, and electronic case report form will be harmonized across participating centers. Second, consecutive eligible patients will be prospectively enrolled before surgery, and MRI and axillary ultrasound features will be recorded before pathological confirmation. Third, the model will be externally assessed for discrimination, calibration, decision-curve net benefit, interobserver reproducibility, and clinical workflow feasibility. The protocol harmonization and reader training phase is expected to be completed within 6 months after ethics approval. Prospective patient enrollment is planned for months 7-24, followed by model performance assessment, calibration analysis, decision-curve analysis, and manuscript preparation during months 25-30. This stepwise validation strategy is necessary before the model can be considered for clinical decision support.

The retrospective management analyses provide context for the potential clinical relevance

of preoperative axillary risk stratification. In this cohort, a high proportion of patients retrospectively categorized as low risk nevertheless underwent invasive axillary procedures under routine clinical practice. At the same time, more extensive axillary surgery was consistently associated with greater perioperative burden, higher postoperative morbidity, worse upper-limb functional outcomes, and increased healthcare utilization. These findings should not be interpreted as evidence that the present model reduced overtreatment in this cohort, because surgical decisions were not based on model output. Rather, they suggest that if a reliable preoperative stratification tool can be validated prospectively, it may help identify clinical scenarios in which the extent of axillary intervention could be further individualized. The 1-year DFS analysis was retained only as a descriptive, hypothesis-generating analysis. Because the number of endpoint events was limited and several treatment subgroups were very small, especially the high-risk patients who did not receive adjuvant therapy, the Cox estimates were unstable. These findings therefore cannot support conclusions regarding adjuvant treatment benefit, treatment selection, or treatment de-escalation.

This study has several limitations. First, this was a single-center retrospective study with a moderate sample size; therefore, selection bias, referral-pattern bias, and information bias cannot be excluded. Second, validation was limited to an internal random split, and the model has not yet been tested in an independent external cohort. The reported validation performance should therefore be regarded as preliminary. Third, the model was derived from treatment-naïve patients only, and its performance in patients receiving neoadjuvant chemotherapy, endocrine therapy, targeted therapy, or immunotherapy remains unknown. Fourth, surgical management in this cohort was determined by routine clinical judgment rather than model output. Therefore, the associations between model-defined risk strata and axillary procedures, postoperative morbidity, or treatment burden should not be interpreted as evidence that the model reduced overtreatment or improved outcomes. Fifth, the 1-year DFS analysis was exploratory and underpowered, with limited endpoint events and very small subgroups in some strata. The survival findings cannot support conclusions regarding treatment benefit or treatment de-escalation. Sixth, although interobserver agreement was good, the model relied on manually interpreted imaging features, and feature assessment may vary across institutions and readers. Finally, the model should be regarded as a preoperative risk-stratification and communication tool rather than a substitute for SLNB, ALND, or pathological confirmation. Prospective multicenter external validation is required before clinical decision support can be considered.

Conclusion

This study showed that spiculated lesion margins on breast MRI, abnormal lymph node hilum structure, nodal microcalcification, higher Adler blood flow grade, and higher RI on axillary ultrasound were associated with ALNM in breast cancer. A CART decision tree derived from these routine imaging features demonstrated acceptable discriminative ability and provided an interpretable framework for preoperative axillary risk stratification. In retrospective analyses, model-defined risk strata were associated with observed patterns of axillary management and short-term postoperative burden. These findings suggest that imaging-based axillary risk stratification may be clinically relevant; however, the model remains exploratory at this stage and requires prospective multicenter external validation before it can be considered for clinical decision support.

Disclosure of conflict of interest

None.

Address correspondence to: Sen Jiang and Yangkang Li, Department of Radiology, Cancer Hospital of Shantou University Medical College, No. 7 Raoping Road, Jinping District, Shantou 515000, Guangdong, China. Tel: +86-0754-8859-9750; E-mail: jansn32888@yeah.net (SJ); liyangkang035@163.com (YKL)

References

[1] Tao X, Li T, Gandomkar Z, Brennan PC and Reed WM. Incidence, mortality, survival, and disease burden of breast cancer in China compared to other developed countries. Asia Pac J Clin Oncol 2023; 19: 645-654.

[2] Wu T, Long Q, Zeng L, Zhu J, Gao H, Deng Y, Han Y, Qu L and Yi W. Axillary lymph node metastasis in breast cancer: from historical axillary surgery to updated advances in the preoperative diagnosis and axillary management. BMC Surg 2025; 25: 81.

[3] Zahwe M, Ghzaiel A, Najia A, Soueid L, El Asmar K, Ghezzawi M, El Iskandarani S, Diab M, El Jibbawi M, Hoteit R and Sbaity E. Performance of sentinel lymph node biopsy after neoadjuvant chemotherapy in clinically node-positive breast cancer patients: systematic review and meta-analysis. Int J Surg 2025; 111: 3040-3050.

[4] Wang W, Qiu P and Li J. Internal mammary lymph node metastasis in breast cancer patients based on anatomical imaging and functional imaging. Breast Cancer 2022; 29: 933-944.

[5] Liu X, Wang M, Wang Q and Zhang H. Diagnostic value of contrast-enhanced ultrasound for sentinel lymph node metastasis in breast cancer: an updated meta-analysis. Breast Cancer Res Treat 2023; 202: 221-231.

[6] Xu K, Wang R, Chen Q, Liu Y, Li X, Mao L, Wang C, Gao F, Hu L, Xie H, Wang C, Zhou G and Guan X. Microenvironment components and spatially resolved single-cell transcriptome atlas of breast cancer metastatic axillary lymph nodes. Acta Biochim Biophys Sin (Shanghai) 2022; 54: 1336-1348.

[7] Zhao Q, Yang F, Wu HL, Mo M, Ling YX and Liu GY. Contralateral axillary lymph node metastasis in breast cancer: an oligometastatic-like disease. Breast 2023; 72: 103589.

[8] Jin Y, Wang W and Li JB. Multi-omics prediction of lymph node metastasis status in breast cancer. Zhonghua Zhong Liu Za Zhi 2024; 46: 391-398.

[9] Im EO, Yi JS and Chee W. A decision tree analysis on symptom experience of Asian American breast cancer survivors. West J Nurs Res 2023; 45: 1076-1084.

[10] Tian JX and Zhang J. Breast cancer diagnosis using feature extraction and boosted C5.0 decision tree algorithm with penalty factor. Math Biosci Eng 2022; 19: 2193-2205.

[11] Gu J, Tong T, Xu D, Cheng F, Fang C, He C, Wang J, Wang B, Yang X, Wang K, Tian J and Jiang T. Deep learning radiomics of ultrasonography for comprehensively predicting tumor and axillary lymph node status after neoadjuvant chemotherapy in breast cancer patients: a multicenter study. Cancer 2023; 129: 356-366.

[12] Zuo D, Yang L, Jin Y, Qi H, Liu Y and Ren L. Machine learning-based models for the prediction of breast cancer recurrence risk. BMC Med Inform Decis Mak 2023; 23: 276.

[13] Ma M, Liu R, Wen C, Xu W, Xu Z, Wang S, Wu J, Pan D, Zheng B, Qin G and Chen W. Predicting the molecular subtype of breast cancer and identifying interpretable imaging features using machine learning algorithms. Eur Radiol 2022; 32: 1652-1662.

[14] Zhang YN, Xia KR, Li CY, Wei BL and Zhang B. Review of breast cancer pathologigcal image processing. Biomed Res Int 2021; 2021: 1994764.

[15] Zhang J, Wu J, Zhou XS, Shi F and Shen D. Recent advancements in artificial intelligence for breast cancer: Image augmentation, segmentation, diagnosis, and prognosis approaches. Semin Cancer Biol 2023; 96: 11-25.

[16] Qi YJ, Su GH, You C, Zhang X, Xiao Y, Jiang YZ and Shao ZM. Radiomics in breast cancer: current advances and future directions. Cell Rep Med 2024; 5: 101719.

[17] Tabár L, Dean PB, Lee Tucker F and Vörös A. Can we improve breast cancer management using an image-guided histopathology workup supported by larger histopathology sections? Eur J Radiol 2023; 161: 110750.

[18] Conti A, Duggento A, Indovina I, Guerrisi M and Toschi N. Radiomics in breast cancer classification and prediction. Semin Cancer Biol 2021; 72: 238-250.

[19] Dołęga-Kozierowski B, Kasprzak P, Lis M, Szynglarewicz B, Matkowski R, Sawicki M, Dymek M, Szumiejko A, Carmo G, Kwiatkowski A, Soliński DG and Ptak M. Numerical and physical modeling of breast cancer based on image fusion and artificial intelligence. Breast Cancer Res Treat 2023; 202: 33-43.

[20] Hou C, Li J, Wang W, Sun L and Zhang J. Second-order asymmetric convolution network for breast cancer histopathology image classification. J Biophotonics 2022; 15: e202100370.

[21] Almalki YE, Soomro TA, Irfan M, Alduraibi SK and Ali A. Impact of image enhancement module for analysis of mammogram images for diagnostics of breast cancer. Sensors (Basel) 2022; 22: 1868.

[22] Jiang S and Colditz GA. Causal mediation analysis using high-dimensional image mediator bounded in irregular domain with an application to breast cancer. Biometrics 2023; 79: 3728-3738.

[23] Nomani A, Ansari Y, Nasirpour MH, Masoumian A, Pour ES and Valizadeh A. PSOWNNs-CNN: a computational radiology for breast cancer diagnosis improvement based on image processing using machine learning methods. Comput Intell Neurosci 2022; 2022: 5667264.

[24] Im EO, Yi JS and Chee W. The characteristics of Asian American breast cancer survivors with low quality of life: a decision tree analysis. J Cancer Educ 2023; 38: 1277-1285.

[25] Wiranata JA, Astari YK, Ucche M, Hutajulu SH, Paramita DK, Sulistyoningrum DC, Siswohadiswasana Y, Asmedi A, Hardianti MS, Taroeno-Hariadi KW, Kurnianda J and Purwanto I. Predictive factors of chemotherapy-induced peripheral neuropathy in breast cancer: a decision tree model approach. JCO Glob Oncol 2024; 10: e2400160.

[26] Gómez Del Moral Herranz RM, López Rodríguez MJ, Seiffert AP, Soto Pérez-Olivares J, Chiva De Agustín M and Sánchez-González P. CureMate: a clinical decision support system for breast cancer treatment. Int J Med Inform 2024; 192: 105647.

[27] Lazarewicz MA, Wlodarczyk D and Johansen Reidunsdatter R. Decision tree analyses for prediction of QoL over a one-year period in breast cancer patients: an added value of patient-reported outcomes. Cancers (Basel) 2023; 15: 2474.

[28] Khalid A, Mehmood A, Alabrah A, Alkhamees BF, Amin F, AlSalman H and Choi GS. Breast cancer detection and prevention using machine learning. Diagnostics (Basel) 2023; 13: 3113.

[29] Im EO, Yi JS and Chee W. A decision tree analysis on the impact of a technology-based program on symptom distress: Asian American breast cancer survivors. Comput Inform Nurs 2022; 40: 487-496.

[30] Xu W, Zheng B, Wen C, Zeng H, Wang S, He Z, Liao X, Chen W, Li Y and Qin G. Enhancing specificity in predicting axillary lymph node metastasis in breast cancer through an interpretable machine learning model with CEM and ultrasound integration. Technol Cancer Res Treat 2025; 24: 15330338251334735.

[31] Tang X, Zhang H, Mao R, Zhang Y, Jiang X, Lin M, Xiong L, Chen H, Li L, Wang K and Zhou J. Preoperative prediction of axillary lymph node metastasis in patients with breast cancer through multimodal deep learning based on ultrasound and magnetic resonance imaging images. Acad Radiol 2025; 32: 1-11.

[32] Wang X, Nie L, Zhu Q, Zuo Z, Liu G, Sun Q, Zhai J and Li J. Artificial intelligence assisted ultrasound for the non-invasive prediction of axillary lymph node metastasis in breast cancer. BMC Cancer 2024; 24: 910.

[33] Agyekum EA, Kong W, Agyekum DN, Issaka E, Wang X, Ren YZ, Tan G, Jiang X, Shen X and Qian X. Ultrasound derived deep learning features for predicting axillary lymph node metastasis in breast cancer using graph convolutional networks in a multicenter study. Sci Rep 2025; 15: 27796.

[34] Giammarile F, Vidal-Sicart S, Paez D, Pellet O, Enrique EL, Mikhail-Lette M, Morozova O, Maria Camila NM, Diana Ivonne RS, Delgado Bolton RC, Valdés Olmos RA and Mariani G. Sentinel lymph node methods in breast cancer. Semin Nucl Med 2022; 52: 551-560.

[35] Reimer T. Omission of axillary sentinel lymph node biopsy in early invasive breast cancer. Breast 2023; 67: 124-128.